SPATIAL PREPROCESSING FOR ENDMEMBER EXTRACTION USING UNSUPERVISED CLUSTERING AND ORTHOGONAL SUBSPACE PROJECTION CONCEPTS

Gabriel Martín and Antonio Plaza

Department of Technology of Computers and Communications
University of Extremadura, Avda. de la Universidad s/n, E-10071 Caceres, Spain
Phone: +34 927 257000 (Ext. 51662) - Fax: +34 927 257203
E-mail: {gamahefpi, aplaza}@unex.es

ABSTRACT

In this paper, we develop a new spatial preprocessing strategy which can be applied prior to a spectral-based endmember extraction process for unmixing of hyperspectral data. Our proposed approach directs the endmember searching process to regions which are both spectrally pure and spatially homogeneous in the scene. Our experimental results, conducted using simulated hyperspectral data sets with known endmembers and fractional abundances, reveal that the proposed approach can successfully integrate the spatial and spectral information in the search for more relevant endmembers.

Index Terms— Spectral unmixing, endmember extraction, spatial-spectral integration.

1. INTRODUCTION

Spectral unmixing is an important task for remotely sensed hyperspectral data exploitation [1]. The spectral signatures collected in natural environments are invariably a mixture of the pure signatures of the various materials found within the spatial extent of the ground instantaneous field view of the imaging instrument. Linear spectral unmixing aims at inferring such pure spectral signatures, called *endmembers*, and the material fractions, called *fractional abundances*, at each pixel of the scene [2]. Let us assume that a remotely sensed hyperspectral scene with n bands is denoted by $\mathbf{I}$, in which the pixel at the discrete spatial coordinates (i, j) of the scene is represented by a vector $\mathbf{X}(i,j) = [x_1(i,j), x_2(i,j), \cdots, x_n(i,j)] \in \Re^n$, where $\Re$ denotes the set of real numbers in which the pixel's spectral response $x_k(i,j)$ at sensor channels $k = 1, \ldots, n$ is included. Under the linear mixture model assumption, each pixel vector in the original scene can be modeled using:

$$\mathbf{X}(i,j) = \sum_{z=1}^{p} \Phi_z(i,j) \cdot \mathbf{E}_z + \mathbf{n}(i,j), \qquad (1)$$

where $\mathbf{E}_z$ denotes the spectral response of endmember z, $\Phi_z(i,j)$ is a scalar value designating the fractional abundance of the endmember z at the pixel $\mathbf{X}(i,j)$, p is the total number of endmembers, and $\mathbf{n}(i,j)$ is a noise vector. Two physical constrains are generally imposed into the model described in Eq. (1), these are the abundance non-negativity constraint (ANC), i.e., $\Phi_z(i,j) \geq 0$, and the abundance sum-to-one constraint (ASC), i.e., $\sum_{z=1}^{p} \Phi_z(i,j) = 1$ [3].

Over the last decade, several algorithms have been developed for automatic or semi-automatic extraction of spectral endmembers [2]. Classic techniques include the pixel purity index (PPI) [4], N-FINDR [5], iterative error analysis (IEA) [6], optical real-time adaptive spectral identification system (ORASIS) [7], vertex component analysis (VCA) [8], and an orthogonal subspace projection (OSP) technique in [9]. These techniques are all based on exploiting the spectral information when searching for image endmembers. However, one of the distinguishing properties of hyperspectral data is the multivariate information coupled with a two-dimensional (pictorial) representation amenable to image interpretation. Subsequently, endmember extraction algorithms could benefit from an integrated framework in which both the spectral information and the spatial arrangement of pixels are considered.

To the best of our knowledge, only a few attempts exist in the literature aimed at including the spatial information in the process of extracting spectral endmembers. Extended morphological operations [10] have been used as a baseline to develop an automatic morphological endmember extraction (AMEE) algorithm [11] for spatial-spectral endmember extraction. Also, spatial averaging of spectrally similar endmember candidates found via singular value decomposition (SVD) was used in the development of the spatial spectral endmember extraction (SSEE) algorithm [12]. Recently, a spatial preprocessing (SPP) algorithm [13] has been proposed which estimates, for each pixel vector in the scene, a spatially-derived factor that is used to weight the importance of the spectral information associated to each pixel in terms of its spatial context. The SPP is intended as a preprocessing module that can be used in combination with an existing spectral-based endmember extraction algorithm. However, this approach relies on the use of a rectangular window of fixed size

which is moved through all the pixels of the image in order to analyze spatial context. This strategy is feasible when spectral variation is smooth and relatively constant over the image but, in order to better model natural scenes with step discontinuities and multi-scale features, further adaptive approaches are needed for the spatial preprocessing stage prior to endmember extraction.

In this paper, we develop a new spatial preprocessing strategy which directs the endmember searching process to regions which are both spectrally pure and spatially homogeneous in the scene. By means of the proposed approach, spatial information is used as a *guide* to exploit spectral information more effectively by adequately exploiting spatial context. Specifically, our proposed approach first adaptively searches for spectrally pure and spatially homogeneous regions by using a hybrid procedure that combines unsupervised clustering and orthogonal subspace projection concepts, thus selecting a set of representative regions in spatial-spectral terms. This preprocessing stage is then followed by a spectral-based endmember extraction process using the pixels located in such regions, which selects only a representative endmember per region. This results in a set of spatially representative endmembers with the potential to accurately characterize large homogeneous areas in the original hyperspectral scene.

2. METHODOLOGY

1. *Feature reduction*. Apply a dimensionality reduction transformation such as principal component analysis (PCA) or minimum noise fraction (MNF) [14] to reduce the dimensionality of the data from n to $p-1$. Here, the value of p is estimated using the virtual dimensionality (VD) concept [15] and the MNF transform is adopted for feature reduction.

2. *Unsupervised clustering*. Clustering aims at grouping pixels if feature space, so that pixels belonging to the same cluster are spectrally similar. In this work, we have used the well-known ISODATA algorithm for this purpose [14]. The algorithm starts with a random initial partition of the available pixel vectors into c candidate clusters, and then reassigns these vectors to clusters in such a way that the squared error is reduced at each iteration, until a convergence criterion is achieved. A relevant issue is how to set the number of clusters c in advance. In this work, this parameter is set to a value that generates an explicit oversegmentation that ideally results in a one-to-many partitioning of scene features into smaller segments. This is because we intend to obtain spatially relevant cluster regions made up of spectrally similar pixel vectors. We have experimentally observed that the regions obtained by setting $c \geq 2p$ generally fulfill the desired properties, but in any event this value can be set as the (only) input parameter.

3. *Intelligent cluster selection*. The main goal of this step is to retain, out of the c clusters resulting from the unsupervised clustering procedure performed in the previous stage, a set of p clusters which are spectrally distinct, with $c \geq p$. For this purpose, we select the more spatially representative region for each cluster (in this work, the connected region with a larger number of pixels) and remove the remaining regions. Then, we select a representative spectral signature for each cluster (in this work, the mean spectral signature of the cluster) and apply the OSP algorithm to find a set of p clusters with representative spectra which are both spectrally pure and orthogonal between them. The OSP starts by identifying the representative spectral signature with higher intensity and labels this signature as the first one in the process [9]. Then, it finds the representative spectral signature which is most orthogonal with regards to the first one, and labels this signature as the second one in the process. Then, it finds the representative spectral signature which is most orthogonal with regards to the first two, and labels this signature as the second one in the process. The procedure is repeated until p representative signatures (associated to p clusters) are extracted. The pixels associated to the remaining $c-p$ clusters –which have not been selected by the cluster selection procedure above– are removed from the original scene.

4. *Endmember extraction*. Finally, a set of endmembers are extracted from the set of pixels associated to the p clusters retained after the intelligent cluster selection procedure above. This is done by applying the OSP procedure again, but this time considering all the pixels associated to the p clusters (instead of only the representative spectral signatures of these clusters) as input to the algorithm. The reason is that spectral averaging generally reduces endmember signature purity and, therefore, it is important to conduct the final endmember search in the original image space, regardless of the fact that averaged spectra were used in the previous step as an effective mechanism to select representative spectra for each cluster region in order to remove regions which are not sufficiently pure. To make sure that only one representative endmember is extracted from each of the p regions, every time that the OSP identifies a pixel in a certain region, all the pixels labeled as belonging to the same region are removed from the original scene. As a result, in the next OSP iteration only the pixels associated to the $p-1$ remaining clusters will be considered as input to the algorithm. At this point, we reiterate that our spectral-based endmember search is conducted in the original image space (from which the pixels associated to regions that are not sufficiently pure have been removed). The output of this step is a

set of p endmembers, which have been intelligently selected taking into account the spatial and the spectral properties of hyperspectral data.

As a final comment, we emphasize that other endmember extraction algorithms such as N-FINDR, IEA or VCA (instead of OSP) can also be used in step 4. As a result, steps 1-3 of the proposed approach can be seen as a spatial preprocessing to a purely spectral-based endmember search conducted in the last step of our methodology.

3. EXPERIMENTAL RESULTS

A preliminary validation of the proposed methodology has been conducted using a simulated hyperspectral scene, created using fractals to generate distinct spatial patterns which are then used to simulate linear mixtures of reflectance signatures selected from a spectral library compiled by the U.S. Geological Survey (USGS)[1]. Fig. 1(a) shows the nine fractional abundance maps used in the generation of the scene, where black color indicates 0% abundance of the corresponding mineral, white color indicates 100% abundance of the mineral, and fractional abundances in each pixel of the scene sum to unity. On the other hand, Fig. 1(b) shows the spectra of the USGS signatures used in the simulation. Of all the mixed pixels (100×100) simulated in the synthetic scene, 41.54% are binary in nature (i.e. made up of two endembers), 20.14% are made up of three endmembers, 18.21% are made up of four endmembers, and 20.08% are made up of five or more endmembers. Zero-mean Gaussian noise was added to the scenes in different signal to noise ratios (SNRs) –from 30:1 to 110:1– to simulate contributions from ambient (clutter) and instrumental sources, following the procedure described in [9].

Fig. 2(a) shows the cluster regions selected after applying steps 1–3 of the proposed algorithm (with $c = 2p$) to the simulated scene with SNR of 30:1. As it can be seen in Fig. 2(a), the regions retained after intelligent cluster selection correspond to spectrally pure regions [i.e., high values in the fractional abundance maps displayed in Fig. 1(a)] which are also spatially representative in the scene. Specifically, the color labeling in Fig. 2(a) is given by the following color-mineral correspondences: blue (*Nontronite*), lime (*Alunite*), cyan (*Sphene*), orange (*Pyropylite*), yellow (*Halloysite*), green (*Muscovite*), purple (*Kaolinite CM9*), pink (*Dumortierite*) and red (*Kaolinite KGa1*). We have experimentally observed that the endmembers extracted from our proposed methodology are very similar, in spectral terms, with regards to the USGS signatures displayed in Fig. 1(b). However, in order to provide quantitative evidence of the potential advantages of the proposed method in terms of spatial-spectral endmember extraction, we consider here a different metric given by the root mean square error (RMSE) in the reconstruction of the original image, which can be defined as follows. Let us assume that $\mathbf{I}^{(\mathrm{O})}$ is the original hyperspectral scene, and that $\mathbf{I}^{(\mathrm{R})}$ is a reconstructed version of $\mathbf{I}^{(\mathrm{O})}$, obtained using Eq. (1) with a set of endmembers and their corresponding ANC and ASC-estimated fractional abundances. Let us also assume that the pixel vector at spatial coordinates (i, j) in the original hyperspectral scene is given by $\mathbf{X}^{(\mathrm{O})}(i,j) = [x_1^{(\mathrm{O})}(i,j), x_2^{(\mathrm{O})}(i,j), \cdots, x_n^{(\mathrm{O})}(i,j)]$, while the corresponding pixel vector at the same spatial coordinates in the reconstructed hyperspectral scene is given by $\mathbf{X}^{(\mathrm{R})}(i,j) = [x_1^{(\mathrm{R})}(i,j), x_2^{(\mathrm{R})}(i,j), \cdots, x_n^{(\mathrm{R})}(i,j)]$. With the above notation in mind, and considering that s is the number of samples and l is the number of lines of the hyperspectral image, the RMSE between the original and the reconstructed images can be calculated as follows:

$$\mathrm{RMSE}(\mathbf{I}^{(\mathrm{O})}, \mathbf{I}^{(\mathrm{R})}) = \frac{1}{s \times l} \sum_{i=1}^{s} \sum_{j=1}^{l} \left(\frac{1}{n} \sum_{k=1}^{n} [x_k^{(\mathrm{O})}(i,j) - x_k^{(\mathrm{R})}(i,j)]^2 \right)^{\frac{1}{2}}. \quad (2)$$

Fig. 2(b-f) graphically represents the per-pixel and global RMSE scores obtained after reconstructing the simulated hyperspectral scene (with different SNR values) using the endmembers extracted by our proposed method, while Fig. 2(g-k) represents the errors obtained after reconstructing the scene using the endmembers extracted by OSP. It can be observed in Fig. 2 that spatial preprocessing allows a significant reduction of RMSE scores, in particular for values of SNR $\geq$50:1. Although these results are quite encouraging, further experiments with real hyperspectral scenes are needed to fully substantiate these observations.

[1] http://speclab.cr.usgs.gov/spectral-lib.htm

4. REFERENCES

[1] J. B. Adams, M. O. Smith, and P. E. Johnson, "Spectral mixture modeling: a new analysis of rock and soil types at the Viking Lander 1 site," *Journal of Geophysical Research*, vol. 91, pp. 8098–8112, 1986.

[2] A. Plaza, P. Martinez, R. Perez, and J. Plaza, "A quantitative and comparative analysis of endmember extraction algorithms from hyperspectral data," *IEEE Trans. Geosci. Remote Sens.*, vol. 42, no. 3, pp. 650–663, 2004.

[3] D. Heinz and C.-I Chang, "Fully constrained least squares linear mixture analysis for material quantification in hyperspectral imagery," *IEEE Trans. Geosci. Remote Sens.*, vol. 39, pp. 529–545, 2000.

[4] J. W. Boardman, F. A. Kruse, and R. O. Green, "Mapping Target Signatures Via Partial Unmixing of Aviris Data," *Proc. JPL Airborne Earth Sci. Workshop*, pp. 23–26, 1995.

[5] M. E. Winter, "N-FINDR: an algorithm for fast autonomous spectral end-member determination in hyperspectral data," *Proc. SPIE Image Spectrometry V*, vol. 3753, pp. 266–277, 2003.

[6] R. A. Neville, K. Staenz, T. Szeredi, J. Lefebvre, and P. Hauff, "Automatic endmember extraction from hyperspectral data for

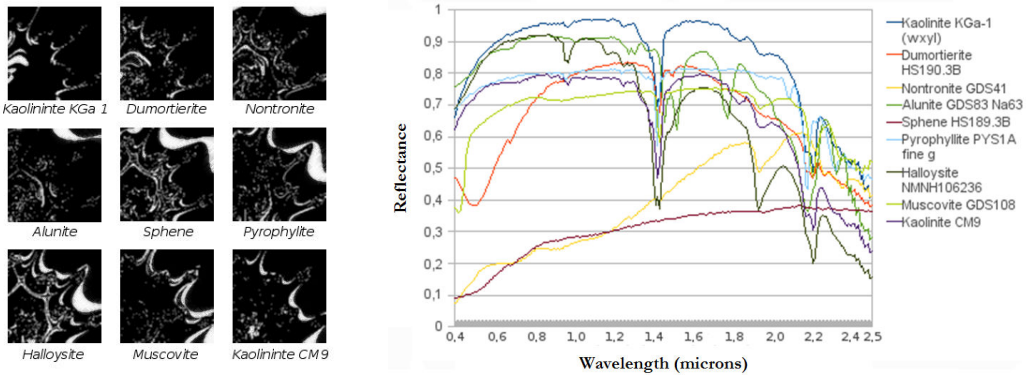

(a) Reference fractional abundances (b) Reference endmember signatures

Fig. 1. (a) Fractional abundance distributions considered for generating the simulated hyperspectral scene used in experiments. (b) USGS library signatures used for the generation of the simulated hyperspectral scene.

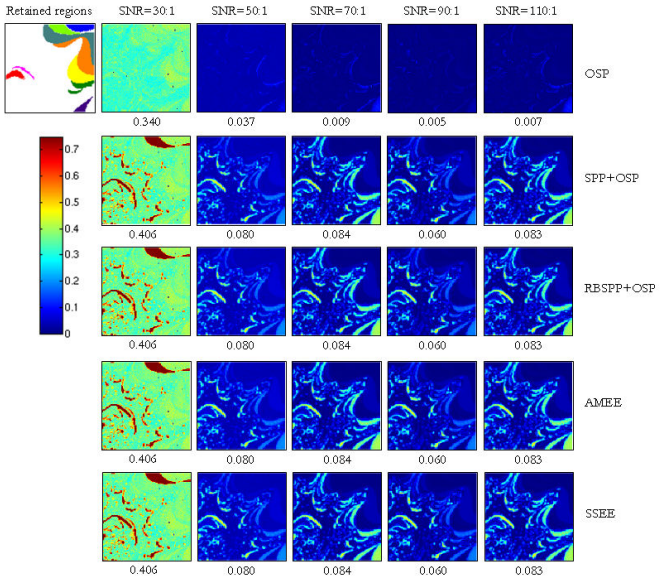

Fig. 2. (a) Cluster regions obtained after applying steps 1–3 of the proposed method to the simulated scene with SNR=30:1. RMSE after reconstructing the simulated scenes with SNR=30:1 (b), SNR=50:1 (c), SNR=70:1 (d), SNR=90:1 (e), and SNR=110:1 (f) using the endmembers extracted by the proposed method. RMSE after reconstructing the simulated scenes with SNR=30:1 (g), SNR=50:1 (h), SNR=70:1 (i), SNR=90:1 (j), and SNR=110:1 (k) using the endmembers extracted by OSP.

mineral exploration," *Proc. 21st Canadian Symp. Remote Sens.*, pp. 21–24, 1999.

[7] J. H. Bowles, P. J. Palmadesso, J. A. Antoniades, M. M. Baumback, and L. J. Rickard, "Use of filter vectors in hyperspectral data analysis," *Proc. SPIE Infrared Spaceborne Remote Sensing III*, vol. 2553, pp. 148–157, 1995.

[8] J. M. P. Nascimento and J. M. Bioucas-Dias, "Vertex component analysis: a fast algorithm to unmix hyperspectral data," *IEEE Trans. Geosci. Remote Sens.*, vol. 43, no. 4, pp. 898–910, 2005.

[9] J. C. Harsanyi and C.-I Chang, "Hyperspectral image classification and dimensionality reduction: An orthogonal subspace projection," *IEEE Trans. Geosci. Remote Sens.*, vol. 32, no. 4, pp. 779–785.

[10] A. Plaza, P. Martinez, J. Plaza, and R. Perez, "Dimensionality reduction and classification of hyperspectral image data using sequences of extended morphological transformations," *IEEE Trans. Geosci. Remote Sens.*, vol. 43, no. 3, pp. 466–479, 2005.

[11] A. Plaza, P. Martinez, R. Perez, and J. Plaza, "Spatial/spectral endmember extraction by multidimensional morphological operations," *IEEE Trans. Geosci. Remote Sens.*, vol. 40, no. 9, pp. 2025–2041, 2002.

[12] D. M. Rogge, B. Rivard, J. Zhang, A. Sanchez, J. Harris, and J. Feng, "Integration of spatial–spectral information for the improved extraction of endmembers," *Remote Sensing of Environment*, vol. 110, no. 3, pp. 287–303, 2007.

[13] M. Zortea and A. Plaza, "Spatial preprocessing for endmember extraction," *IEEE Trans. Geosci. Remote Sens.*, vol. 47, pp. 2679–2693, 2009.

[14] J. A. Richards and X. Jia, *Remote Sensing Digital Image Analysis: An Introduction*, Springer, 2006.

[15] C.-I Chang and Q. Du, "Estimation of number of spectrally distinct signal sources in hyperspectral imagery," *IEEE Trans. Geosci. Remote Sens.*, vol. 42, no. 3, pp. 608–619, 2004.